Epoxidized Block and Statistical Copolymers Reinforced by Organophosphorus−Titanium−Silicon Hybrid Nanoparticles: Morphology and Thermal and Mechanical Properties

Faezeh Hajiali, Saeid Tajbakhsh, and Milan Marić*

ACCESS | Metrics & More | Article Recommendations | Supporting Information

ABSTRACT: Glycidyl methacrylate (GMA) and a mixture of alkyl methacrylates (average chain length of 13 carbons; termed C13MA; derived from vegetable oils) were copolymerized by nitroxide-mediated polymerization to form epoxidized statistical and block copolymers with similar compositions (F_{GMA} ∼0.8), which were further cross-linked by a bio-based diamine. Hybrid plate-like nanoparticles containing organophosphorus−titanium−silicon (PTS) with an average size of ∼130 nm and high decomposition temperature (485 °C) were synthesized via a hydrothermal reaction to serve as additives to simultaneously enhance the thermal and mechanical properties of the blend. Nanocomposites filled with PTS were prepared at different filler-loading levels (0.5, 2, 4 wt %). Transmission electron microscopy (TEM) of the cured block copolymer displayed reaction-induced macrophase-separated domains. TEM also showed an effective dispersion of PTS hybrids in the matrix without intense agglomeration. Thermogravimetric analysis at different heating rates revealed the activation energy of poly (GMA-$stat$-C13MA) at maximum decomposition increased from 143.5 to 327.2 kJ mol^{-1} with 4 wt % PTS. Decomposition temperature and char residue improved 12 °C and ∼7 wt %, respectively, and T_g increased 12 °C by adding 4 wt % PTS. Targeting various PTS concentrations enabled tuning of the tensile modulus (up to 75%), tensile strength (up to 46%), and storage modulus in both glassy state (up to 59%) and rubbery plateau regions (up to 88%). Oscillatory frequency sweeps indicated that PTS makes the storage modulus frequency dependent, suggesting that the inclusion of the nanoparticles alters the relaxation of the surrounding matrix polymer.

Cross-linked Poly(GMA-$stat$-C13MA) + PTS

Cross-linked Poly(GMA-b-C13MA) + PTS
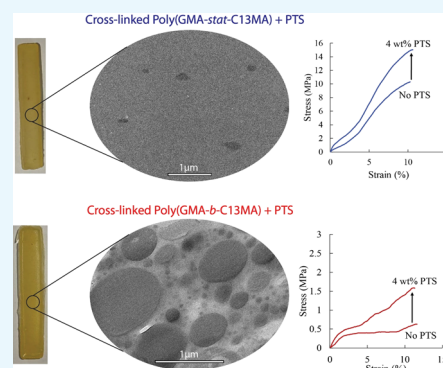
1. INTRODUCTION

Polymers impart flexibility and desirable mechanical, electrical, and thermal properties to a myriad of products, but they also require flammability reduction and thermal stability improvement to be adopted for those applications. Various inherently thermally stable polymers like fluoropolymers and poly-(vinylchloride) are often substituted by more flammable polymers because of recycling challenges, costs, or environmental concerns for the elimination of certain compounds such as heavy metals or halogens in materials waste.[1,2] In this context, the fabrication of polymer nanocomposites filled with organic−inorganic hybrid nanoadditives compatible with the polymer matrix for thermostability enhancement with fewer environmental repercussions has warranted considerable attention.[3]

To date, a large number of nanofillers, including carbon materials,[4,5] phosphoric compounds,[6−9] siliceous compounds,[10−13] and minerals,[14−16] have been used to improve both thermal and mechanical properties of polymers. Nano-additives can be applied at much lower concentrations (<10 wt %) compared to traditional fillers with markedly observed enhancement in mechanical properties, conductivity, and solvent resistance.[17,18] This is due to the "nano-effect" causing changes in the local properties of the matrix and the small distances between nanofillers particles even at low mass loadings along with an extremely high surface area of nanofillers.[18] For instance, the addition of 1 wt % rod-shaped carbon nanofibers (∼200 nm in diameter) in polyurethane foams simultaneously improved thermal degradation onset by 18 °C and enhanced flexural modulus from 143 to 207 MPa.[19] Incorporating polyhedral oligomeric silsesquioxanes (POSS) at low loadings into epoxy resins not only increased the limiting oxygen index (LOI) by ∼7% but also improved the oxidation resistance of the resin.[20,21] In a recent study, we showed that POSS nanoparticles improved both tensile modulus (from 96 to 179 MPa) and thermal decomposition temperature (225−255 °C) in recyclable thermosets based on vinylogous urethane cross-linking networks.[22] Addition of clay to polymers contributes to long-term thermo-oxidative stability
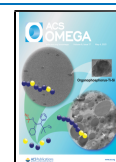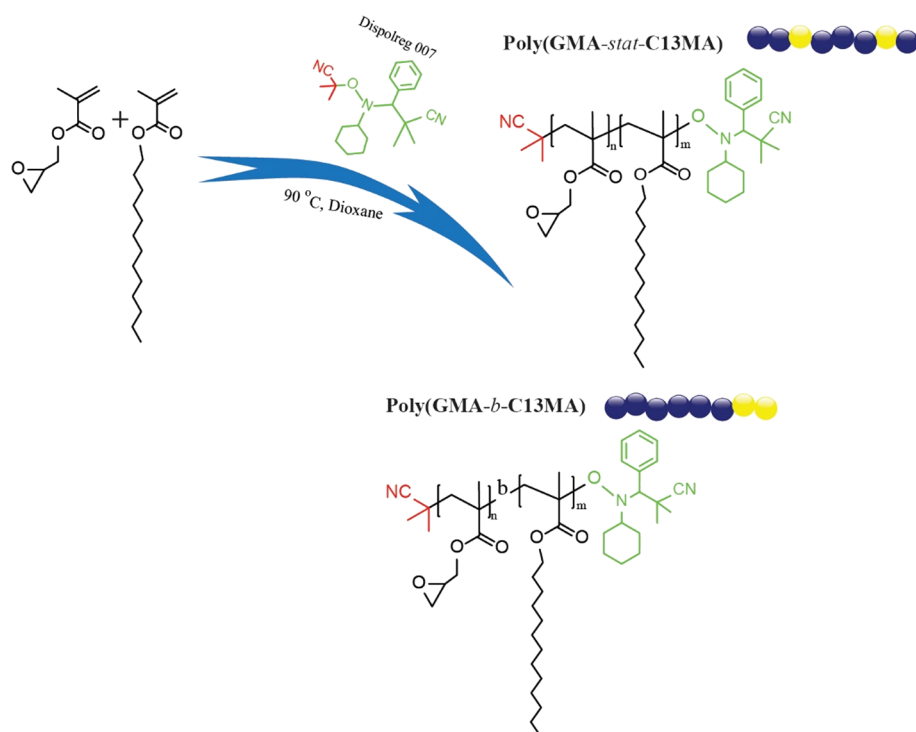
Figure 1. NMP scheme of poly(GMA-*stat*-C13MA) and poly(GMA-*b*-C13MA) using Dispolreg 007.

and thermal stability since clay can act as both a heat insulator and a mass transport barrier to oxygen and the volatiles generated during the degradation.[23,24]

During the past several years, hybridization of inorganic—organic materials has brought a new perspective to the development of high-performance materials.[25,26] Incorporation of inorganic—organic nanoadditives has been widely used for improving the thermal stability of polymers because of the synergistic effect between their inorganic and organic components.[27] In addition, the presence of organic moieties plays an important role in the morphology, dispersity, and thermal stability of such hybrid nanofillers.[28−30] Organophosphorus compounds, such as ammonium polyphosphate[31] and diphenylphosphinic acid[32] have been used as inorganic additives for improving the thermal stability and flame resistance of polymeric materials. There have been several studies concerning hybrid nanomaterials such as aluminum—organophosphorus,[30] phosphorus-doped silica,[33,34] silica—graphene oxide,[35,36] and silica—carbon[37] that have exhibited marked thermostability. For instance, only 2 wt % of Cu_2O-TiO_2-GO nanosheets reduced the heat release rate of unsaturated polyester by ~30%.[38] Epoxy resin reinforced with 5 wt % Ti-Si exhibited 13 °C increase in glass transition temperature (T_g), 16 °C increase in decomposition temperature, and enhanced storage modulus compared to pure epoxy.[39] Recently, Wei et al.[40,41] reported hybrid nanofillers that contained organophosphorus—titanium—silicon (PTS) to fabricate high performance flame-retardant polycarbonate. Only 0.1 wt % of the nanoparticles endowed polycarbonate with a LOI of 29.7%, 8% improvement in tensile strength, and 8.3% improvement in elongation at break. Such an improvement in both mechanical and thermal stability was ascribed to the uniform dispersion of PTS and suitable interfacial interactions with the polymeric matrix.

Inspired by Wei et al.[40,41] we prepared organic—inorganic hybrid PTS nanoparticles with a lower organophosphorus content. We used PTS to simultaneously enhance the mechanical and thermal stability properties of epoxy-functionalized methacrylate thermosets. We synthesized statistical and block copolymers with a similar composition of glycidyl methacrylate (GMA) and bio-based C13 methacrylate (C13MA, from vegetable oils) using nitroxide-mediated controlled radical polymerization (NMP) (Figure 1). Since the incorporation of vegetable oil-derived monomers in the polymer chains affects the strength of GMA, we decided to reinforce the copolymer by adding low amounts of PTS with potential applications in adhesive and antiflammable coatings. We targeted statistical copolymers to introduce epoxy functionality randomly throughout the chain while a block copolymer was used to introduce localized epoxy segments. Previously, many efforts have been devoted to toughen epoxy resins with various renewable polymer additives such as triscardanyl phosphate[42] and bio-based polymers derived from castor oil,[43] vanillin,[44] and soybean oil.[45] Additionally, the synthesis of copolymers containing long chain alkyl methacrylates provides low-T_g, soft, and elastic domains capable of sustaining deformation through viscous flow and chain entanglements.[46−48] Thus, in the present study, we incorporated a low concentration (~20 mol %) of a rubbery phase (C13MA, whose polymer has a $T_g \sim -45$ °C) to increase the toughness of GMA. The synthesized polymers were then converted to thermosets via an epoxy-amine cross-linking reaction using a dimeric amine. Finally, the influence of incorporation of PTS on the morphology, and thermal, mechanical and rheological properties was investigated and discussed accordingly.

2. EXPERIMENTAL SECTION

2.1. Materials. Tetrabutyl titanate (TBT, 97%), tetraethyl orthosilicate (TEOS, 99%), diphenylphosphinic acid (DPPA, 98%) and 1,4-dioxane (≥99.9%) were purchased from Millipore-Sigma. GMA (Sigma, 97%) and C13 methacrylate (C13MA, a mixture of alkyl methacrylates (∼C10−C16), Evonik) were passed through a column of basic alumina to remove the inhibitors. 3-(((2-Cyanopropan-2-yl) oxy) - (cyclohexyl) amino)-2 and 2-dimethyl-3-phenylpropanenitrile (Dispolreg 007) initiator were synthesized following Ballard et al.'s method.[49] Priamine 1075 was received from Croda. Ethanol, toluene, tetrahydrofuran (HPLC, ≥99.9%), and methanol were purchased from Fisher Scientific. Deuterated chloroform (CDCl$_3$) was received from Cambridge Isotopes Laboratory.

2.2. Polymer Synthesis. We synthesized statistical and block copolymers of GMA and bio-based C13MA with similar compositions by NMP. For poly(GMA-*stat*-C13MA), GMA (54.0 g, 0.38 mol), C13MA (25.5 g, 0.09 mol), Dispolreg 007 (0.90 g, 2.65 mmol), and dioxane (80.5 g) were added to a 250 mL three-neck flask. After purging the solution with nitrogen for 30 min it was heated at 90 °C for 4.5 h. Samples taken during the reaction were analyzed by gel permeation chromatography (GPC) and proton nuclear magnetic resonance (^{1}H NMR) spectroscopy. At the end of the reaction, the solution was precipitated into methanol and dried in vacuum at room temperature for 24 h. For the synthesized poly(GMA-*stat*-C13MA), the final conversion was 65%, Đ = 1.52, M_n = 21.8 kg mol^{-1}, and F_{GMA} = 0.81.

To prepare poly(GMA-*b*-C13MA), we first synthesized the poly(GMA) macroinitiator by adding GMA (40.0 g, 0.28 mol), Dispolreg 007 (0.4 g, 1.18 mmol), and dioxane (40 g) to a flask and after purging with nitrogen, the solution was heated at 90 °C for 1.5 h (X = 32%). After precipitation from methanol, the product was dried in a vacuum oven overnight. For the poly(GMA) macroinitiator, M_n = 19.1 kg mol^{-1} and Đ = 1.55. Next, poly(GMA) (14.1 g, 0.73 mmol), C13MA (10.8 g, 0.04 mol), and dioxane (24.9 g) were added into a 125 mL flask and the same procedure at 90 °C was followed and the reaction took 3 h. For the synthesized poly(GMA-*b*-C13MA), the final conversion was 32%, M_n = 25.3 kg mol^{-1}, Đ = 1.87, and F_{GMA} = 0.83.

2.3. Nanoparticle Synthesis. Following the approach by Wei et al.,[40,41] we synthesized PTS nanoparticles by applying the same method but with a lower organic content to decrease the decomposition at high temperatures, which resulted in different nanoparticle structures. We first added TBT (6.66 mmol) and TEOS (6.66 mmol) in a mixed solution of ethanol/deionized water (0.13 mol/0.13 mol) containing a few drops of acetyl acetone to prevent the hydrolysis of TBT. After 1 h, DPPA (6.66 mmol) was added and mixed in the Ti-Si sol gel, and the mixture was transferred to an oven at 160 °C for 12 h. Finally, the product was washed sequentially with ethanol, deionized water, ether, and acetone followed by drying in a vacuum oven at 80 °C overnight.

2.4. Nanocomposite Synthesis. We prepared poly-(GMA-*stat*-C13MA)/PTS and poly(GMA-*b*-C13MA)/PTS nanocomposites by a solvent casting method. The sample ID and formulation of nanocomposites are provided in Table 1. As an example, for S-2 which contains 2 wt % PTS, poly(GMA-*stat*-C13MA) (4.0 g, M_n = 21.8 kg mol^{-1}, and F_{GMA} = 0.81) was first dissolved in toluene (4.0 g). In a

Table 1. Formulation of Poly(GMA-*stat*-C13MA)/PTS and Poly(GMA-*b*-C13MA)/PTS Nanocomposites

sample ID	polymer (wt %)	PTS (wt %)
S-0	poly(GMA-*stat*-C13MA) (100)	0
S-0.5	poly(GMA-*stat*-C13MA) (99.5)	0.5
S-2	poly(GMA-*stat*-C13MA) (98)	2
S-4	poly(GMA-*stat*-C13MA) (96)	4
B-0	poly(GMA-*b*-C13MA) (100)	0
B-4	poly(GMA-*b*-C13MA) (96)	4

separate vial, PTS nanoparticles (80.3 mg) were dispersed in toluene (4.0 g) by sonication using a Hielscher sonicator UP200S (50% duty cycle and amplitude 70%) for 15 min and then added to the polymer. The sonicated energy employed for nanoparticle dispersion can be obtained according to the literature.[50] The polymer solution containing PTS nanoparticles was stirred for 10 min followed by adding cross-linker solution (0.8 g of Priamine 1075 in 1.0 g of toluene) and further stirring for 1−2 min. The prepared mixture was cast into the silicone molds with rectangular, dumbbell, and circular shaped molds. The samples were dried and cured at room temperature for 5 days and then post-cured in an oven at 40 °C under vacuum for 6 h to ensure full dryness and curing. Figure S1 shows the picture of the cured nanocomposites.

2.5. Measurements. The characterization of the synthesized polymers in terms of molecular weight (M_n) and dispersity Đ was carried out using GPC (Waters Breeze) with tetrahydrofuran (HPLC grade) as the eluent at 40 °C at a flow rate of 0.3 mL min^{-1} with polymethyl methacrylate (PMMA) standards. Three Waters HR Styragel GPC columns equipped with a guard column were used. More details on the instrument and the columns were given previously.[51] Dynamic light scattering (DLS) was conducted using a Malvern Zetasizer Nano ZS equipped with a 4 mW He−Ne laser at 633 nm and an avalanche photodiode detector. The measurement was conducted at 25 °C at 173° angle on diluted samples (concentration of 0.01−1000 mg mL^{-1}). X-Ray photoelectron spectroscopy (XPS) was conducted using a Fischer Scientific Kα spectrometer using a spot size of 200 μm, running 5 survey scans at 200 mV for 50 ms residence times, and 10 scans for 50 ms residence times for specific elements. Differential scanning calorimetry (DSC, Q2000, TA Instruments) and thermogravimetric analysis (TGA, Q500, TA Instruments) were performed at a rate of 10 °C min^{-1} under nitrogen using aluminum pans. ^{1}H NMR spectra were recorded using a Varian NMR Mercury spectrometer at 32 scans and 300 MHz with deuterated chloroform solvent. Fourier transform infrared spectroscopy (FTIR) spectra were obtained using a Bruker Alpha FTIR. Dynamic mechanical analysis (DMA) and rheology measurements were performed using an Anton Paar MCR 302 in dynamic oscillatory mode (0.1−100 Hz, amplitude 1%) with a CTD 450 oven and 25 mm parallel plate geometry under nitrogen at 100 °C. DMA was carried out on rectangular-shaped samples (60 mm length, 10 mm width and 2 mm thickness) at a rate of 5 °C min^{-1} and a frequency of 1 Hz. Tensile testing was performed using an MTS Insight material testing system on dumbbell-shaped specimens (ASTM D638 type V, length = 60 mm, width = 10 mm) at a cross-head speed of 10 mm min^{-1} and a 5 kN load cell. Transmission electron microscopy (TEM) of nanocomposites and the neat PTS were carried out on ultramicrotome-cut 1 μm-thick sections on conductive grids without chemical staining using Thermo
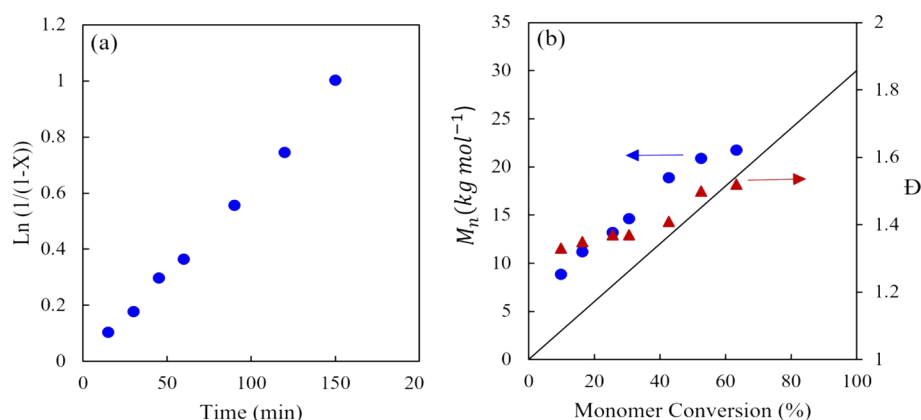
Figure 2. NMP of GMA/C13MA at 90 °C in dioxane solvent: (a) semi-logarithmic kinetic plot of $\ln[1/(1-X)]$ (X = monomer conversion) versus reaction time and (b) M_n, and Đ versus conversion. For the final poly(GMA-*stat*-C13MA), final X = 65%, Đ = 1.52, M_n = 21.8 kg mol^{-1}, and F_{GMA} = 0.81.

Scientific Talos F200X G2 (S/TEM) at an acceleration voltage of 200 kV. This instrument allowed high-angle annular dark-field (HAADF) in scanning mode (STEM) images to be achieved with improved contrast within the macrophase-separated material.

3. RESULTS AND DISCUSSION

3.1. Synthesis and Characterization of Poly(GMA-*stat*-C13MA) and Poly(GMA-*b*-C13MA). We targeted methacrylate-based statistical and block copolymers containing epoxy functional groups, which are widely used in coatings.[52,53] We adopted NMP and synthesized poly(GMA-*stat*-C13MA) using Dispolreg 007 initiator at 90 °C with a high initial GMA fraction, $f_{GMA,0}$ 0.8 and targeting $M_{n,theo}$ = 30 kg mol^{-1} (molecular weight at 100% conversion). As shown in Figure 2, the plot of monomer conversion versus time revealed pseudo first-order kinetics of both C13MA and GMA. In addition, the growth of polymer molecular weight remained consistent with monomer conversion and Đ was consistently low (1.33 < Đ <1.52), superficially indicating a controlled polymerization.

In addition to the synthesis of poly(GMA-*stat*-C13MA), we also prepared a diblock copolymer by NMP. We intentionally targeted a low C13MA concentration for the second block to achieve a similar overall composition to the statistical copolymer. Using this approach, a poly(GMA) macroinitiator (M_n = 19.1 kg mol^{-1}, Đ = 1.55) was synthesized beforehand, which then initiated the polymerization of C13MA leading to poly(GMA-*b*-C13MA). After precipitation into methanol, the block copolymer was characterized by GPC to indicate that the second block had successfully grown from the macroinitiator. Figure 3 presents a moderate shift of M_n toward higher molecular weights because of the relatively high M_n of the poly(GMA) macroinitiator and the small poly(C13MA) segment. The high Đ = 1.87 is due to the low molecular weight tail indicative of some dead macroinitiator present. We carried out multiple Gaussian peak fitting for the macroinitiator to roughly estimate the fraction of dead polymer chains. According to the fitting analysis in Figure S2, 13% of the macroinitiator chains were estimated to be dead. We discussed the effect of the dead chains and high Đ on the morphology of the block copolymer in Section 3.3.

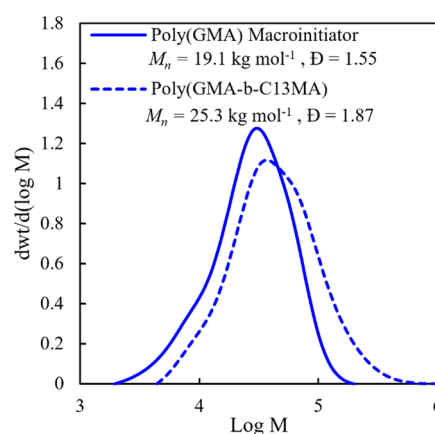**3.2. Characterization of Synthesized PTS.** DLS, TGA, FTIR, and TEM were used to characterize the synthesized PTS

Figure 3. GPC chromatogram of the poly(GMA) macro-chain transfer agent and poly(GMA-*b*-C13MA) diblock copolymer (THF eluent at 0.3 mL min^{-1} with PMMA standards at 40 °C).

nanoparticles. Figure 4a shows the average particle size of PTS ~130 nm, obtained from DLS. TGA of PTS in Figure 4b indicates a very low weight loss (<10%) as heating increased from 50 to 485 °C which could be attributed to the release of bound water in nanoparticles. With increasing temperature, PTS starts to decompose through a single-step decomposition with a DTG peak appearing at about 560 °C which is mainly involved in the degradation of organic functional groups (organophosphorus moieties) and ultimately having a relatively high residue (54.6% at 800 °C).[54,55] The chemical structure of PTS was analyzed by FTIR as shown in Figure 4c. Peaks at 1088 and 1050 cm^{-1} correspond to the Ti-O-P and Si-O-P, respectively. Additionally, the vibration peaks of Si-O and Ti-O exist at 795 and 566 cm^{-1}.[41,56] The peak around 3500 cm^{-1} is ascribed to H_2O. To further analyze the structure of PTS, XPS was performed. Figure S3a shows the peaks located at 533.0, 458.8, 284.6, 132.7, and 103.6 eV in the XPS spectrum, corresponding to O 1 s, Ti 2p, C 1 s, P 2p, and Si 2p, respectively. Figure S3b shows the P 2p XPS spectra of the nanoparticles with three peaks at 132.1, 132.7, and 133.4 eV corresponding to P-C, P-O-Ti, and P-O-Si, respectively.

The microstructure of PTS hybrid nanoparticles was further investigated by TEM. Figure 5a,b shows the TEM micrographs of PTS which indicate PTS nanoparticles formed irregular amorphous aggregated structures, ranging from 70 to 170 nm
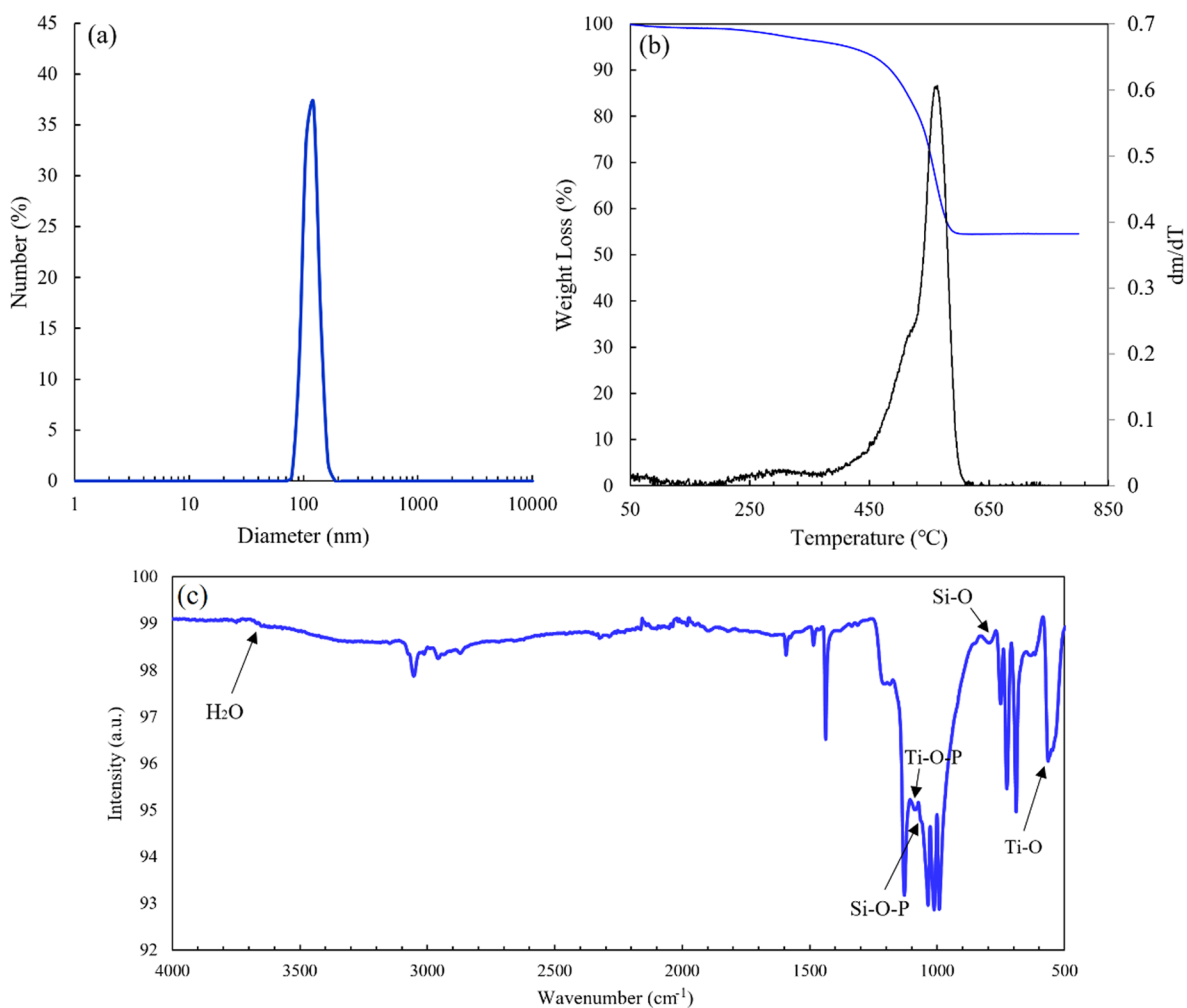
Figure 4. (a) DLS, (b) TGA, and (c) FTIR spectra of the synthesized PTS hybrid nanoparticles.
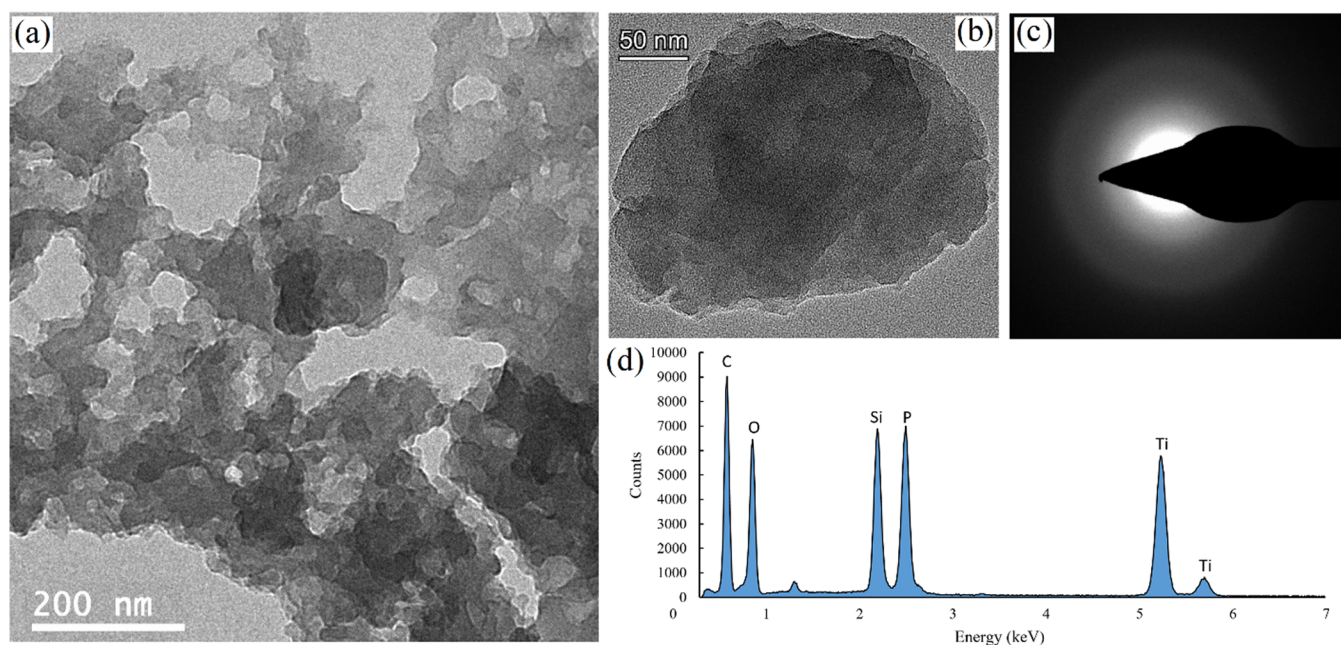

Figure 5. (a, b) TEM images of the hybrid PTS dispersed in toluene, (c) SAED pattern, (d) EDX result of PTS.

in size. Such irregular microstructures of hybrid nanoparticles were previously observed and deemed to be platelet-like.[57−59]

This was not as noticeable due to the aggregates caused by the concentrated solution we applied prior to TEM observation.
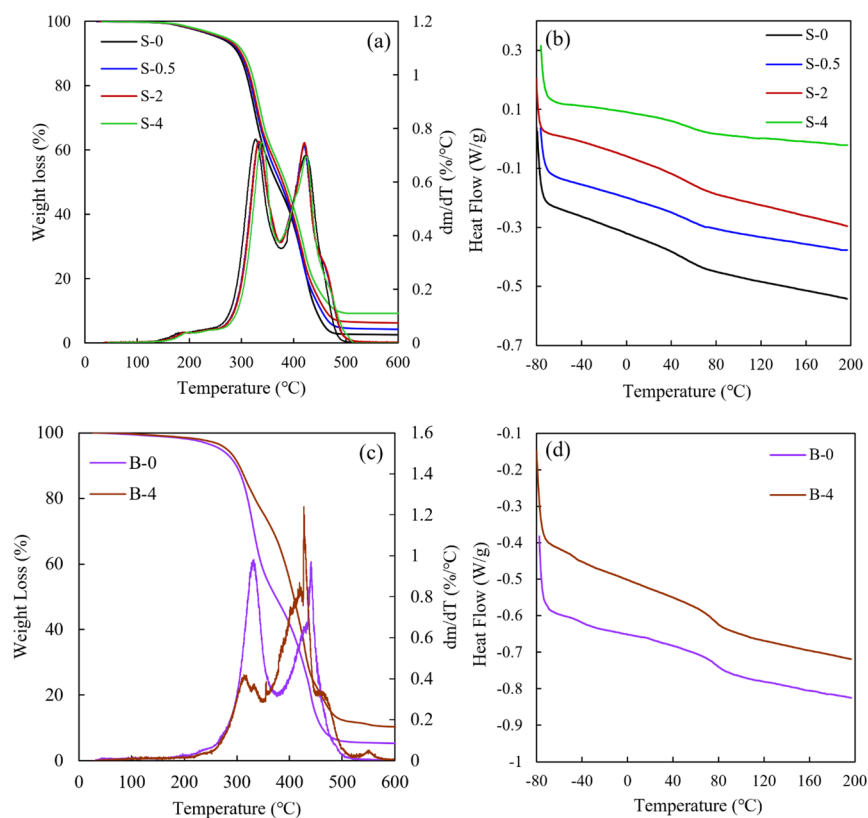
Figure 6. Influence of PTS on TGA and DSC of cured (a, b) poly(GMA-*stat*-C13MA) and (c, d) poly(GMA-*b*-C13MA).

Table 2. Thermal Characterization of Poly(GMA-*stat*-C13MA) and Poly(GMA-*b*-C13MA) Cured Polymers and Nanocomposites

ID	polymer	PTS (wt %)	F_{GMA}	T_g (°C)	$T_{10\%}$ (°C)	$T_{max,1}$ (°C)/$T_{max,2}$ (°C)	residue at 600 °C (%)
S-0	poly(GMA-*stat*-C13MA)	0	0.81	65	293	317/404	2.5
S-0.5	poly(GMA-*stat*-C13MA)	0.5	0.81	69	298	326/407	4.2
S-2	poly(GMA-*stat*-C13MA)	2	0.81	74	300	331/415	6.3
S-4	poly(GMA-*stat*-C13MA)	4	0.81	77	305	337/421	9.2
B-0	poly(GMA-*b*-C13MA)	0	0.83	−39, 84	298	328/430	4.9
B-4	poly(GMA-*b*-C13MA)	4	0.83	−33, 91	304	325/426	10.1

Figure 5c presents a typical selected area electron diffraction (SAED) pattern for PTS without any diffraction spots or rings observed, indicating an amorphous structure. Further, the elemental composition of PTS was probed by EDX. The EDX results confirmed that P and C both exist in PTS besides the Si, Ti, and O, confirming the formation of hybrid nanoparticles (Figure 5d).

3.3. Influence of PTS on the Thermal Behavior of Poly(GMA-*stat*-C13MA) and Poly(GMA-*b*-C13MA). The thermal stability of poly(GMA-*stat*-C13MA) and poly(GMA-*b*-C13MA) was evaluated by TGA (Figure 6a,c) under nitrogen. The TGA thermograms for all the nanocomposites exhibit a two-step degradation at 330 and 400 °C. The weight losses observed at lower temperatures are attributed to the decomposition of side chains of polymers while those at higher temperatures are attributed to main-chain degradation.[60,61] According to Table 2, the onset degradation temperature increased 12 °C from cured, unloaded poly(GMA-*stat*-C13MA) (S-0) to the 4 wt % PTS-reinforced nanocomposite (S-4). Additionally, there was an increase in the maximum decomposition temperatures from 317 and 404 °C to 337 and 421 °C, respectively, indicating an improvement in the thermal

stability of the nanocomposites. These enhancements in thermal stability are due to the incorporation of thermally stable PTS into poly(GMA-*stat*-C13MA) where the polymer-nanoparticle interaction is strong.[62] As a comparison, the addition of 1 wt % TiO$_2$, nanoclay, and carbon nanofibers to polyurethane improved the decomposition temperature by 7.1, 15.6, and 17.6 °C, respectively.[19] Furthermore, the residual weight percentage at the conclusion of the TGA tests increased from 2.5 to 9.2 wt %, which is the sum of the inorganic compounds plus the char products from the polymer.[54] In the case of block copolymers, the onset degradation temperature increased 6 °C and the residual weight percentage increased by 5.2 wt % from B-0 to B-4.

DSC curves shown in Figure 6b,d show that the glass transition temperature (T_g) for the poly(GMA-*stat*-C13MA) nanocomposite increased from 65 °C (for S-0) to 77 °C (for S-4) with increasing concentration of PTS from 0 to 4 wt %, which indicates that the interaction of polymer chains was enhanced by the incorporation of thermally stable PTS. The uniform dispersion of PTS in the polymer (Section 3.5) restricts the mobility of polymer chains which enhances the T_g of the polymer.[63,64] The literature T_gs of the rubbery

poly(C13MA) and rigid poly(GMA) are −45 °C[51,65] and 83 °C,[66] respectively. In the case of block copolymers, the epoxy groups of GMA in poly(GMA-*b*-C13MA) were able to react with amine end groups of Priamine, so that the block copolymer could cure within the epoxy network with the possibility of microphase separation.[67,68] The microphase separation of poly(GMA-*b*-C13MA) was observed by DSC. According to Figure 6d, two different T_g values at approximately −40 and ~85 °C were detected for poly-(GMA-*b*-C13MA) corresponding to the poly(C13MA) and poly(GMA) blocks, respectively. To confirm microphase separation of poly(GMA-*b*-C13MA), we estimated the total solubility parameters for C13MA (δ= 15.43 MPa$^{1/2}$) and GMA (δ= 19.25 MPa$^{1/2}$) from Hansen solubility parameters.[69] The Hansen solubility parameters of lauryl methacrylate were used to roughly estimate the total solubility parameter, δ, for C13MA as the information for C13MA was not available. The difference in estimated solubility parameters indicates the immiscibility between the poly(C13MA) and poly(GMA) blocks. After adding PTS into diblock copolymer, both T_g peaks shifted toward higher temperatures, increasing by 6 and 7 °C for the poly(GMA) and poly(C13MA) block segments, respectively, compared to the cured poly(GMA-*b*-C13MA), which was observed for similar block copolymer nanocomposites in the literature.[70]

The cross-linked poly(GMA-*b*-C13MA), B-0, was examined for phase separation behavior by HAADF-STEM (Figure 7) to
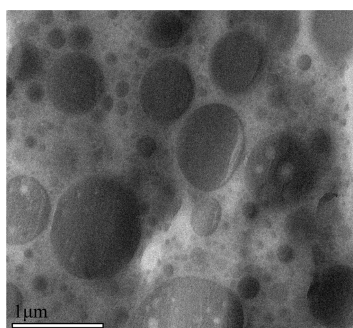

Figure 7. HAADF-STEM micrographs of cross-linked poly(GMA-*b*-C13MA) (B-0). Darker domains are due to increased density which is attributed to the cross-linked GMA segments.

give contrast depending on the mass density. On the basis of previous studies demonstrating that polymers with higher density have dark contrast by HAADF,[71,72] we propose that the darker regions correspond to the cross-linked GMA segments. The observation of phase-separation based on different mass densities has been previously reported in nonreactive block copolymers[73,74] and cross-linked block copolymers.[75−77]

The HAADF-STEM image of B-0 demonstrated macrophase-separated domains on scales larger than that expected for microphase separated block copolymer length scales (~ several radii of gyration (R_g) of the polymers, R_g ~ 10−50 nm), which could be ascribed to reaction-induced macrophase separation, where the structures of several nanometers to microns can be formed via spinodal decomposition and/or nucleation and growth mechanisms.[78−80] In reaction-induced macrophase separation, there is a competition between the curing speed and mobility (viscosity) at a given temperature, resulting in phase-separated structures with domain lengths ~

several hundred nanometers.[78,81] In such systems, it is essential to use a good diluent (nonreactive solvent) to attain a homogeneous mixture and subsequently remove the solvent. If the solvent is not evaporated rapidly, the viscosity of the system could be low enough to allow an increase in the nanodomain coarsening rate. This may in turn affect the morphology dimensions and eventually lead to macrophase separation.[82,83] Macrophase-separated epoxidized polymers are usually characterized by opacity because of the light scattering of separated domains with dimensions comparable to the wavelength of visible light. The images of B-0 and S-0 provided in Figure S4 indicate the opacity of the cured poly(GMA-*b*-C13MA) compared to the transparent poly(GMA-*stat*-C13MA). It should be noted that according to Section 3.1, the diblock copolymer (B-0) in the present study contains a blend of a low fraction of dead poly(GMA) chains and poly(GMA-*b*-C13MA) chains. Solubilizing the diblock copolymer in toluene before the addition of the cross-linker provides a high mobility and the C13MA block remains free for the macrophase to separate. After the addition of Priamine, the mobility of the C13MA block is inhibited by the rigidity of the cured epoxy groups.[78] For comparison, Grubbs et al.[80] obtained opaque samples with macrophase-separated thermosets using polyisoprene-block-poly(methyl acrylate-co-glycidyl acrylate) copolymers and 4,4′-methylenedianiline hardener. They observed that the macrophase-separated domains were greater than 100 nm to millimeter-scale regions.[80] The incorporation of rubbery modifiers or block copolymers as toughening agents can lead to the formation of macro-phase separated structures in epoxy resins.[78,84] For instance, Pearson et al.[85] observed large multiphase particles (10 μm) with "salami"-type structures at 15 phr rubber content in butadiene-acrylonitrile modified epoxy resin. Additionally, very small (approximately 0.1 μm) particles populated the interstitial space between the large particles.[85]

3.4. Influence of PTS on the Thermal Degradation Kinetics of Poly(GMA-*stat*-C13MA). The thermal degradation kinetics of poly(GMA-*stat*-C13MA) and the influence of PTS on the degradation kinetics was investigated by TGA at different heating rates to be further evaluated by Kissinger's method.[86,87] According to Figure 8a,b, the heating rate has a great effect on the thermal stability, i.e., the higher heating rate, the higher the thermal stability.[88] In fact, the characteristic temperature point would move to a higher value by increasing the heating rate.[89] Kissinger's method can be applied to determine the activation energy without a precise knowledge of the degradation mechanism.[90] The activation energy at the maximum decomposition rate was thus obtained by using the following equation:

$$\ln\left(\frac{\beta}{T_{max}^2}\right) = \ln\frac{AR}{E} + \ln[n(1-\alpha_{max})^{n-1}] - \frac{E}{RT_{max}} \quad (1)$$

where T_{max} is the absolute temperature, α_{max} is the conversion at the maximum weight-loss rate, A is the pre-exponential factor, β is the heating rate, E is the activation energy, and R is the universal gas constant. Figure 8c shows the calculation of activation energy from graphs of $\ln\left(\frac{\beta}{T_{max}^2}\right)$ versus $\frac{1}{T_{max}}$ at heating rates of 5, 10, 15, and 20 °C/min according to eq 1. According to Figure 8c, the activation energy of poly(GMA-*stat*-C13MA) at α_{max} increased from 143.5 to 327.2 kJ mol^{-1} with the addition of 4 wt % PTS. This could be due to the interactions
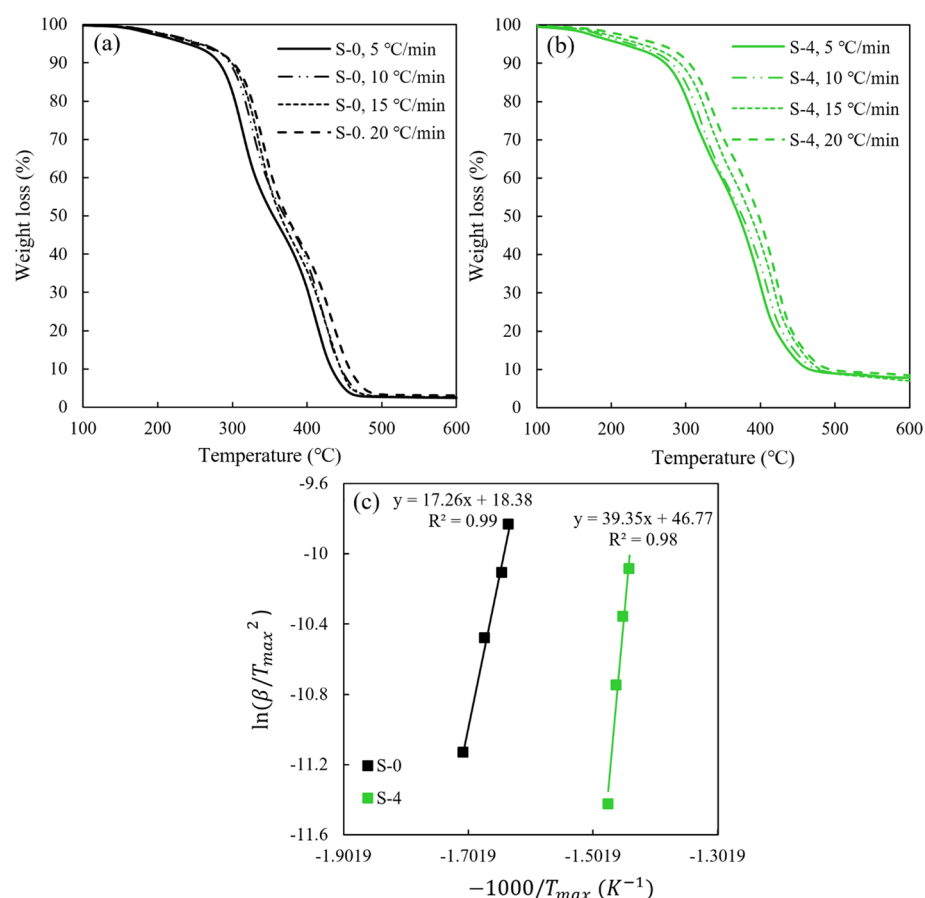
Figure 8. TGA curves of (a) cured poly(GMA-*stat*-C13MA) (S-0) and (b) nanocomposite (S-4) at different heating rates, (c) Kissinger plots for S-0 and S-4.

Table 3. Effects of PTS on the Tensile Properties of Poly(GMA-*stat*-C13MA) and Poly(GMA-*b*-C13MA)

ID	polymer	PTS (wt %)	Young's modulus (MPa)	stress at break (MPa)	strain at break (%)
S-0	poly(GMA-*stat*-C13MA)	0	71.13 ± 7.25	10.29 ± 0.70	10.29 ± 1.91
S-0.5	poly(GMA-*stat*-C13MA)	0.5	87.08 ± 5.69	11.19 ± 0.44	10.15 ± 0.94
S-2	poly(GMA-*stat*-C13MA)	2	103.15 ± 1.22	14.04 ± 0.11	11.13 ± 1.34
S-4	poly(GMA-*stat*-C13MA)	4	124.01 ± 5.59	15.03 ± 1.11	10.61 ± 1.23
B-0	poly(GMA-*b*-C13MA)	0	14.05 ± 0.21	0.76 ± 0.12	11.74 ± 0.83
B-4	poly(GMA-*b*-C13MA)	4	17.02 ± 0.32	1.59 ± 0.23	11.21 ± 0.33

between the nanoparticles and the escaping moieties during degradation which provide a mass transport barrier against volatile degradation products and increases the activation energy.[91] The increase in activation energy also indicates an improvement in the formation of thermally stable char by PTS nanoparticles.[90] For comparison, the average values of activation energy for neat epoxy and epoxy/graphene oxide (GO) are 57 and 65 kJ mol^{-1}, which means that the introduction of GO slows down the degradation reactions.[92] In another study, the presence of polythiophene increased the activation energy of epoxy resin at α_{max} from 165.6 to 221.6 kJ mol^{-1}.[93] In the case of poly(methacrylates), the activation energies of PMMA degradation increased at high degradations (above 40%, $\alpha > 0.4$) by the incorporation of 5 wt % silica nanoparticles.[91]

3.5. Mechanical and Rheological Behavior and Morphology of the Nanocomposites. The tensile properties for cured statistical and block copolymers (S-0 and B-0) and their composite counterparts with different filler loadings

are summarized in Table 3. A comparison between the tensile properties of cured statistical and block copolymers, S-0 and B-0, reveals significantly lower Young's modulus and stress at break in B-0 (14.05 and 0.76 MPa, respectively) compared to S-0 (71.13 and 10.29 MPa, respectively). The lower glass transition temperature (−45 °C) of the soft segment and difference in morphologies contribute to lower modulus and stress at break of B-0 at room temperature. This could be also due to the un-cross-linked poly(C13MA) segment attached to the cross-linked poly(GMA) segment instead of being dispersed randomly with GMA.[94] In fact, the poly(C13MA) soft segment block acts like a plasticizer as previously observed with other C13MA-containing copolymers.[51] Additionally, the tensile modulus taken from the initial linear region of the stress−strain curve depends on the total crystallinity,[95] thus, a lack of soft-segment crystallizability under strain and the possibility of phase separation could limit the tensile properties of the soft-segment-based block copolymer.[96] On the contrary, the presence of covalent cross-linking bonds throughout the
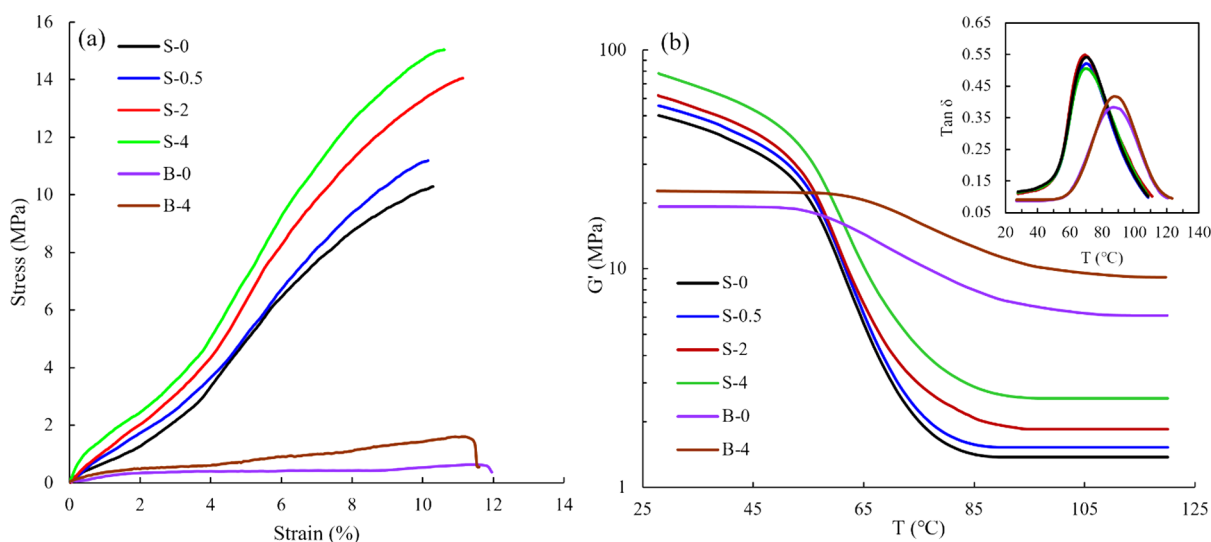
Figure 9. Effects of PTS on (a) tensile properties and (b) dynamic mechanical properties of cured poly(GMA-*stat*-C13MA) (S-0) and poly(GMA-*b*-C13MA) (B-0).
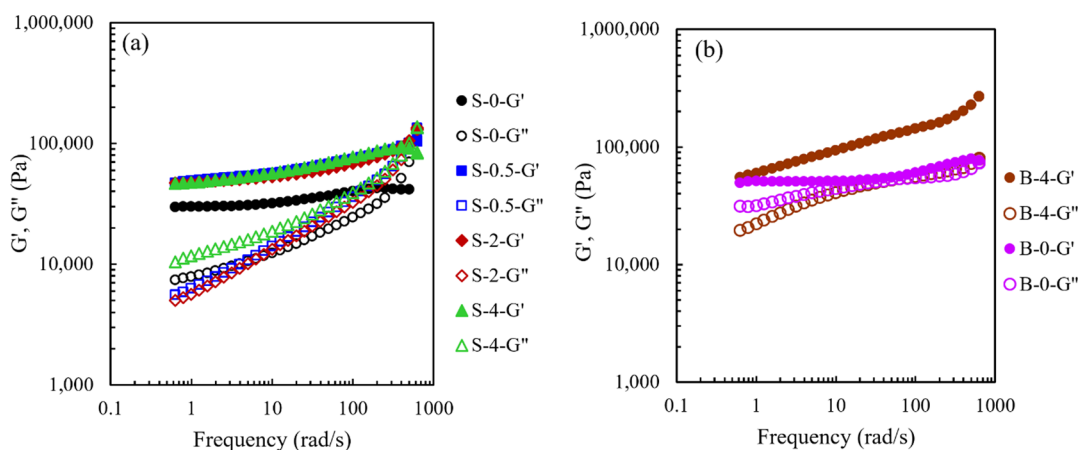

Figure 10. G′ (storage modulus) and G″ (loss modulus) versus frequency of (a) cured poly(GMA-*stat*-C13MA) (S-0) and (b) poly(GMA-*b*-C13MA) (B-0) and their nanocomposites with different filler loadings under nitrogen at 100 °C.

polymer chains in the statistical copolymer results in the reduction in the mobility of whole polymer chains. However, the C13MA segments in the block copolymer are attached to the rigid GMA segments at only one end and therefore are not restricted as much.[97] This consequently slightly increases the elongation observed of the poly(GMA-*b*-C13MA) block copolymer compared to the poly(GMA-*stat*-C13MA) statistical copolymer.

Figure 9a shows representative tensile stress versus strain curves. Among statistical copolymers and composites (samples S-0, S-0.5, S-2, and S-4), the highest increase in tensile modulus is 74% (from 71.13 to 124.01 MPa) and tensile strength is 46% (from 10.29 to 15.03 MPa) at 4 wt % PTS loading. Essentially, the strain at break is about the same and slightly increases at the loading of 2 wt % (from 10.29 to 11.13%) and decreases slightly to 10.61% with further increasing the PTS content. For the block copolymers (samples B-0 and B-4), we observed a 21% increase in tensile modulus and 109% increase in tensile strength. The elongation at break of the B-4 nanocomposite decreases slightly from 11.74 to 11.21%. For comparison, the tensile modulus and strength of epoxy/GO nanocomposites with 0.5 wt % GO

increased from 3.15 ± 0.11 to 3.36 ± 0.17 GPa (6%) and 52.98 ± 5.82 to 64.79 ± 4.01 MPa (22%), respectively, compared to the neat epoxy resin.[98] Bortz et al.[99] showed that the addition of 0.1 wt % GO in epoxy resin yielded a 12% increase in tensile modulus. Melt-mixing addition of 7 wt % multiwall carbon nanotubes in styrene−butadiene−styrene triblock copolymers improved the tensile strength of the nanocomposite by 66%.[70] 3 wt % TiO$_2$/polyurethane nanocomposites had ~15% improvement in tensile strength compared to the cured polymer counterpart.[100] According to Buxton et al.[101] rod and plate type particles provide better mechanical reinforcement in polymer matrices compared to spherical nanoparticles. Among the anisotropic nanoparticles, plate-like nanoparticles provide higher mechanical reinforcement than nanorods as they have a propensity to orient to the tensile direction.[101,102]

DMA probed the thermomechanical effects of PTS incorporation in poly(GMA-*stat*-C13MA) and poly(GMA-*b*-C13MA). For S-0 to S-4 specimens, targeting various PTS concentrations enabled tuning of the storage modulus in both the glassy state (up to 59%) and rubbery plateau regions (up to 88%), as shown in Figure 9b. The storage modulus in the
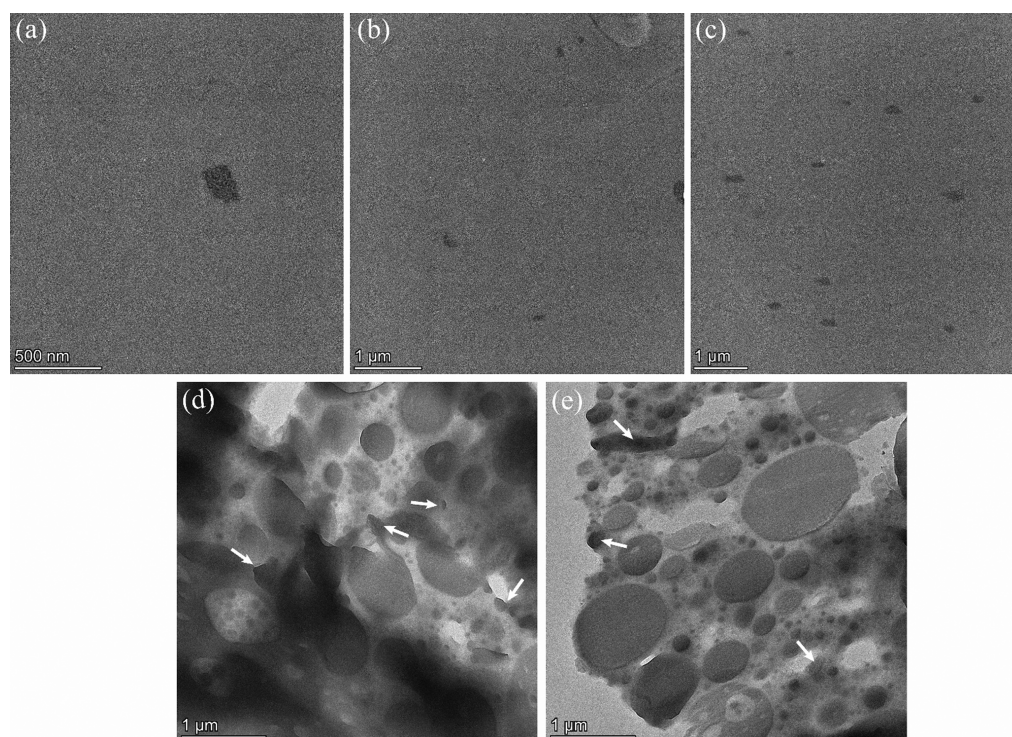
Figure 11. HAADF-STEM of cross-linked poly(GMA-*stat*-C13MA) and poly(GMA-*b*-C13MA) containing PTS hybrids: (a) S-0.5, (b) S-2, (c) S-4, and (d,e) B-4 (small white arrows indicate PTS).

glassy region mainly depends on the stiffness of the filler, good dispersion of filler, and polymer-filler interactions.[41] The damping factor (tan δ, indicative of T_g) shifted toward higher temperatures and became slightly less intense at higher PTS concentrations because of interactions between PTS and the surrounding polymer network. This is in good agreement with the evidence derived from DSC and TGA experiments. B-0 and B-4 samples exhibited very different dynamic mechanical behavior at temperatures above 25 °C because of macrophase structures (data below room temperature are not available). Generally, the DMA of phase-separated copolymers in the full temperature range covering both T_gs displays two distinct transitions; one at a lower temperature corresponding to the glass−rubber transition of the elastomeric soft phase and the other at higher temperatures related to the transition of the rigid phase.[103,104] In the present study, both B-0 and B-4 samples exhibited neither a sharp drop in G′ nor a real plateau at high temperatures. This behavior is in good agreement with previous studies on DMA behavior of block copolymers.[105,106] The damping factor is less pronounced than the statistical copolymers, corresponding to the transition of the rigid poly(GMA) phase (second T_g). Although the data for the glassy region are not available, we can generally conclude that PTS increases the modulus, as the rigid particles stiffen the network.

Frequency sweep measurements were carried out to better understand how PTS interacts with the polymer network. The elastic modulus (G′) and loss modulus (G″) of cured poly(GMA-*stat*-C13MA) and poly(GMA-*b*-C13MA) and their nanocomposite counterparts are shown in Figure 10. As expected, G′ of PTS-filled systems is substantially higher than G′ of the neat counterparts. Figure 10 shows small increases in G′ of the PTS-filled blends while the G′ of S-0 and B-0 do not significantly increase with frequency. In all cases, the

dependence of G″ on frequency is more pronounced and increases substantially (around an order of magnitude) with frequency. Since the frequency dependence of G′ has been observed for other cross-linked nanocomposites,[107,108] we concluded that the G′ of PTS nanocomposites is frequency dependent and it seems that the PTS might physically interact with the polymer chains. This observation implies that at low frequencies, the polymer chains have enough time to relax after deformation which results in lower modulus.[109] However, at high frequencies (>10 rad/s) the polymer chains do not have enough time to relax, and thus the modulus increases. The neat thermosets however do not show a substantial frequency dependence of G′ within the range measured, indicating the covalently cross-linked network structures.[107] As observed in Figure 10, for S-0, S-0.5, S-2, and S-4 samples, the storage modulus at low frequencies up ∼10 rad/s is roughly an order of magnitude higher than the loss modulus. In the case of B-4, this occurs at higher frequencies (above 50 rad/s).

As the dispersion and the interfacial interaction of nanoparticles could markedly affect the mechanical properties of the polymer, the dispersion of PTS nanoparticles was investigated by HAADF-STEM. Figure 11 shows the thin slices of the nanocomposites. For S-0.5, S-2, and S-4 samples, the dispersion of PTS particles can be clearly observed in Figure 11 without intense agglomeration. Additionally, the shape of nanoparticles is the same as that shown in Figure 5 and there is no obvious gap between the polymer and PTS, showing a blurred interface. Additionally, a comparison between Figure 11d,e and Figure 7 shows that the incorporation of PTS did not alter the morphology of the cured block copolymer blend. Indeed, the poly(GMA-*b*-C13MA) nanocomposites consisted of the same macrophase-separated morphology as the network without any nanoparticles. Similarly, in a study by Esposito et al.,[110] the morphology of an epoxidized poly(styrene-*b*-

butadiene-b-styrene) copolymer remained unaltered after the incorporation of carboxylic acid-modified MWCNTs. Based on the STEM results, we can conclude that the interfacial compatibility between PTS and the synthesized polymer was sufficient to disperse the particles, without obvious agglomeration of the nanoparticles.

Overall, DMA, TGA, and tensile testing showed that the addition of PTS more effectively improved the thermal and mechanical properties of the cured poly(GMA-stat-C13MA) compared to the cured poly(GMA-b-C13MA). This could be attributed to the dispersion of the PTS in the statistical and block copolymer matrix. Previous studies have shown that the dispersion of nanoparticles in the block copolymers is complicated due to the phase separation behavior.[111,112] In fact, the competition between the macrophase separation of the block copolymer and the aggregation of the nanoparticles determines the size of aggregates and the ultimate structure of the nanocomposites. Since the mechanical properties and thermal stability did not improve in B-4 as much as it did in S-4, it can be concluded that NP dispersion is reduced in the block copolymer because of the formation of phase-separated domains.[111,113,114] However, we still chose to study nanoparticle dispersion in the block copolymers as preferential segregation of the nanoparticles in one of the domains could enhance a property such as thermal stability or barrier enhancement.

4. CONCLUSIONS

Epoxy-functional copolymers (statistical and segmented block) were synthesized by NMP with potential applications in adhesive and antiflammable coatings. PTS hybrids were added to enhance the thermal and mechanical properties, simultaneously. For the cured block copolymer, microphase separation was verified by the appearance of two T_gs. The TEM micrographs of the cured poly(GMA-b-C13MA) showed dispersed spherical microdomains in a range of ∼100−500 nm because of the reaction-induced macrophase separation upon curing. PTS hybrid nanoparticles were synthesized via a hydrothermal reaction with the average size of 130 nm, $T_{10\%}$ = 485 °C, 55% residue at 800 °C, and plate-like structures, and were further incorporated in the polymers to improve the thermal stability and mechanical properties. DSC revealed that T_g of poly(GMA-stat-C13MA) nanocomposites increased from 65 to 77 °C by adding 4 wt % PTS. TGA showed that $T_{10\%}$ and char residue was enhanced, up to 12 °C and ∼7 wt %, respectively. The activation energy of poly(GMA-stat-C13MA) at α_{max} increased from 143.5 to 327.2 kJ mol^{-1} with the addition of 4 wt % PTS. In addition to thermal stability, tensile modulus and tensile strength increased from 71.13 to 124.01 MPa and 10.29 to 15.03 MPa, respectively, upon the addition of 4 wt % PTS. Further, storage modulus improved in both the glassy region (up to 59%) and the rubbery plateau region (up to 88%). We concluded PTS sufficiently interacted with the host resin as it was effectively dispersed into the resin, based on the TEM, mechanical, and rheological measurements. Overall, these PTS hybrids indicate some promise as modifiers in polymer resins with enhanced thermal stability.

ASSOCIATED CONTENT

Supporting Information

The Supporting Information is available free of charge at https://pubs.acs.org/doi/10.1021/acsomega.1c00993.

Formulation of PTS-incorporated nanocomposites; results of multiple Gaussian fitting for estimation of dead polymer chains; XPS spectra of PTS; and images of Cured Poly(GMA-stat-C13MA) and Poly(GMA-b-C13MA) (PDF)

AUTHOR INFORMATION

Corresponding Author

Milan Marić − Department of Chemical Engineering, McGill University, Montreal, Quebec H3A 0C5, Canada; orcid.org/0000-0002-4984-8761; Email: milan.maric@mcgill.ca

Authors

Faezeh Hajiali − Department of Chemical Engineering, McGill University, Montreal, Quebec H3A 0C5, Canada; orcid.org/0000-0003-1739-3966

Saeid Tajbakhsh − Department of Chemical Engineering, McGill University, Montreal, Quebec H3A 0C5, Canada; orcid.org/0000-0003-4177-3272

Complete contact information is available at:
https://pubs.acs.org/10.1021/acsomega.1c00993

Notes

The authors declare no competing financial interest.

REFERENCES

(1) Higginbotham, A. L.; Lomeda, J. R.; Morgan, A. B.; Tour, J. M. Graphite Oxide Flame-Retardant Polymer Nanocomposites. *ACS Appl. Mater. Interfaces* **2009**, 1, 2256−2261.

(2) Nam, K.-H.; Jin, J.-U.; Lee, J. H.; Kim, J.; Chung, Y. S.; Yeo, H.; You, N.-H.; Ku, B.-C. Highly efficient thermal oxidation and cross-linking reaction of catechol functionalized polyacrylonitrile copolymer composites for halogen-free flame retardant. *Compos. Part B: Eng.* **2020**, 184, No. 107687.

(3) Kumar, A. P.; Depan, D.; Singh Tomer, N.; Singh, R. P. Nanoscale particles for polymer degradation and stabilization—Trends and future perspectives. *Prog. Polym. Sci.* **2009**, 34, 479−515.

(4) Du, C.; Li, M.; Cao, M.; Feng, S.; Guo, H.; Li, B. Enhanced thermal and mechanical properties of polyvinlydene fluoride composites with magnetic oriented carbon nanotube. *Carbon* **2018**, 126, 197−207.

(5) Ren, Y.; Zhang, Y.; Fang, H.; Ding, T.; Li, J.; Bai, S.-L. Simultaneous enhancement on thermal and mechanical properties of polypropylene composites filled with graphite platelets and graphene sheets. *Compos. Part A Appl. Sci. Manuf.* **2018**, 112, 57−63.

(6) Wang, Z.; Huang, Z.; Li, X.; Zhou, J.-A. A nano graphene oxide/α-zirconium phosphate hybrid for rigid polyvinyl chloride foams with simultaneously improved mechanical strengths, smoke suppression, flame retardancy and thermal stability. *Compos. Part A Appl. Sci. Manuf.* **2019**, 121, 180−188.

(7) Lin, Y.; Tyler, R.; Sun, H.; Shi, K.; Schiraldi, D. A. Improving oxygen barrier property of biaxially oriented PET/phosphate glass composite films. *Polymer* **2017**, *127*, 236−240.

(8) Qiu, S.; Zhou, Y.; Ren, X.; Zou, B.; Guo, W.; Song, L.; Hu, Y. Construction of hierarchical functionalized black phosphorus with polydopamine: A novel strategy for enhancing flame retardancy and mechanical properties of polyvinyl alcohol. *Chem. Eng. J.* **2020**, *402*, No. 126212.

(9) Hajiali, F.; Tajbakhsh, S.; Marić, M. Thermal characteristics and flame retardance behavior of phosphoric acid-containing poly (methacrylates) synthesized by RAFT polymerization. *Mater. Today Commun.* **2020**, *25*, No. 101618.

(10) Hajiali, F.; Marić, M. Incorporation of POSS to improve thermal stability of bio-based polymethacrylates by nitroxide-mediated polymerization: Polymerization kinetics and characterization. *J. Polym. Sci.* **2020**, *58*, 1503−1520.

(11) Yin, R.; Cheng, H.; Hong, C.; Zhang, X. Synthesis and characterization of novel phenolic resin/silicone hybrid aerogel composites with enhanced thermal, mechanical and ablative properties. *Compos. Part A Appl. Sci. Manuf.* **2017**, *101*, 500−510.

(12) Sangthumchai, T.; Kamjornsupamitr, T.; Saengsaen, S.; Pumingdawn, N.; Panawong, C.; Sumranjit, J.; Budsombat, S. Composite polymer electrolyte membranes from semi-interpenetrating networks of poly (vinyl alcohol) and silica nanoparticles containing poly (2-acrylamido-2-methyl-1-propanesulfonic acid). *Polymer* **2020**, No. 122910.

(13) Tajbakhsh, S.; Hajiali, F.; Marić, M. Incorporation of methacryloisobutyl POSS in bio-based copolymers by nitroxide mediated polymerization in organic solution and miniemulsion. *J. Appl. Polym. Sci.* **2021**, *138*, No. 50095.

(14) Meng, W.; Dong, Y.; Li, J.; Cheng, L.; Zhang, H.; Wang, C.; Jiao, Y.; Xu, J.; Hao, J.; Qu, H. Bio-based phytic acid and tannic acid chelate-mediated interfacial assembly of Mg(OH)2 for simultaneously improved flame retardancy, smoke suppression and mechanical properties of PVC. *Compos. Part B: Eng.* **2020**, *188*, No. 107854.

(15) Luo, X.; Shen, J.; Ma, Y.; Liu, L.; Meng, R.; Yao, J. Robust, sustainable cellulose composite aerogels with outstanding flame retardancy and thermal insulation. *Carbohydr. Polym.* **2020**, *230*, No. 115623.

(16) Jin, L.; Huang, Q.-J.; Zeng, H.-Y.; Du, J.-Z.; Xu, S. Organic modification of Mo-decorated MgAl layered double hydroxide for polymer flame retardancy. *Compos. Part A Appl. Sci. Manuf.* **2020**, *129*, No. 105717.

(17) Vaia, R. A.; Maguire, J. F. Polymer Nanocomposites with Prescribed Morphology: Going beyond Nanoparticle-Filled Polymers. *Chem. Mater.* **2007**, *19*, 2736−2751.

(18) Paul, D. R.; Robeson, L. M. Polymer nanotechnology: nanocomposites. *Polymer* **2008**, *49*, 3187−3204.

(19) Saha, M. C.; Kabir, M. E.; Jeelani, S. Enhancement in thermal and mechanical properties of polyurethane foam infused with nanoparticles. *Mater. Sci. Eng., A* **2008**, *479*, 213−222.

(20) Ye, X.; Zhang, W.; Yang, R.; He, J.; Li, J.; Zhao, F. Facile synthesis of lithium containing polyhedral oligomeric phenyl silsesquioxane and its superior performance in transparency, smoke suppression and flame retardancy of epoxy resin. *Compos. Sci. Technol.* **2020**, *189*, No. 108004.

(21) Shi, H.; Yang, J.; You, M.; Li, Z.; He, C. Polyhedral Oligomeric Silsesquioxanes (POSS)-Based Hybrid Soft Gels: Molecular Design, Material Advantages, and Emerging Applications. *ACS Mater. Lett.* **2020**, *2*, 296−316.

(22) Hajiali, F.; Tajbakhsh, S.; Marić, M. Thermally reprocessable bio-based polymethacrylate vitrimers and nanocomposites. *Polymer* **2021**, *212*, No. 123126.

(23) Dintcheva, N. T.; Al-Malaika, S.; Morici, E. Novel organo-modifier for thermally-stable polymer-layered silicate nanocomposites. *Polym. Degrad. Stabil.* **2015**, *122*, 88−101.

(24) Kiliaris, P.; Papaspyrides, C. D. Polymer/layered silicate (clay) nanocomposites: an overview of flame retardancy. *Prog. Polym. Sci.* **2010**, *35*, 902−958.

(25) Sharma, P.; Nebhani, L. Hybrid polymers based on bio-based benzoxazines with inorganic siloxane linkage to confer impressive thermal performance. *Polymer* **2020**, No. 122549.

(26) Wang, H.; Qian, C.; Liu, J.; Zeng, Y.; Wang, D.; Zhou, W.; Gu, L.; Wu, H.; Liu, G.; Zhao, Y. Integrating Suitable Linkage of Covalent Organic Frameworks into Covalently Bridged Inorganic/Organic Hybrids toward Efficient Photocatalysis. *J. Am. Chem. Soc.* **2020**, *142*, 4862−4871.

(27) Qiu, S.; Xing, W.; Feng, X.; Yu, B.; Mu, X.; Yuen, R. K. K.; Hu, Y. Self-standing cuprous oxide nanoparticles on silica@ polyphosphazene nanospheres: 3D nanostructure for enhancing the flame retardancy and toxic effluents elimination of epoxy resins via synergistic catalytic effect. *Chem. Eng. J.* **2017**, *309*, 802−814.

(28) Cho, B.-G.; Lee, J.-E.; Hwang, S.-H.; Han, J. H.; Chae, H. G.; Park, Y.-B. Enhancement in mechanical properties of polyamide 66-carbon fiber composites containing graphene oxide-carbon nanotube hybrid nanofillers synthesized through in situ interfacial polymerization. *Compos. Part A Appl. Sci. Manuf.* **2020**, *135*, No. 105938.

(29) Tajbakhsh, S.; Marić, M. Nitroxide mediated miniemulsion polymerization of methacryloisobutyl POSS: Homopolymers and copolymers with alkyl methacrylates. *J. Polym. Sci.* **2020**, *58*, 2741−2754.

(30) Jiajun, M.; Junxiao, Y.; Yawen, H.; Ke, C. Aluminum−organophosphorus hybrid nanorods for simultaneously enhancing the flame retardancy and mechanical properties of epoxy resin. *J. Mater. Chem.* **2012**, *22*, 2007−2017.

(31) Qiu, S.; Ma, C.; Wang, X.; Zhou, X.; Feng, X.; Yuen, R. K. K.; Hu, Y. Melamine-containing polyphosphazene wrapped ammonium polyphosphate: A novel multifunctional organic-inorganic hybrid flame retardant. *J. Hazard. Mater.* **2018**, *344*, 839−848.

(32) Wang, X.; Guo, W.; Cai, W.; Wang, J.; Song, L.; Hu, Y. Recent advances in construction of hybrid nano-structures for flame retardant polymers application. *Appl. Mater. Today* **2020**, *20*, No. 100762.

(33) Zhang, J.; Zhou, X.; Tang, J.; Ren, Y.; Jiang, M.; Tang, Y.; Wang, H.; Yang, J. Phosphoric acid induced homogeneous crosslinked phosphorus doped porous Si nanoparticles with superior lithium storage performance. *Appl. Surf. Sci.* **2020**, *509*, No. 144873.

(34) Wang, B.; Xu, Y.-J.; Li, P.; Zhang, F.-Q.; Liu, Y.; Zhu, P. Flame-retardant polyester/cotton blend with phosphorus/nitrogen/silicon-containing nano-coating by layer-by-layer assembly. *Appl. Surf. Sci.* **2020**, *509*, No. 145323.

(35) Qi, Z.; Shi, J.; Zhang, Z.; Cao, Y.; Li, J.; Cao, S. PEGylated graphene oxide-capped gold nanorods/silica nanoparticles as multifunctional drug delivery platform with enhanced near-infrared responsiveness. *Mater. Sci. Eng. C* **2019**, *104*, No. 109889.

(36) Wang, Z.-G.; Yang, Y.-L.; Lan, R.-T.; Dai, K.; Duan, H.-J.; Lei, J.; Xu, L.; Xu, J.-Z.; Li, Z.-M. Significantly enhanced thermal conductivity and flame retardance by silicon carbide nanowires/graphene oxide hybrid network. *Compos. Part A Appl. Sci. Manuf.* **2020**, *139*, No. 106093.

(37) Chen, L.; Zheng, J.; Fu, R. Hybrid nanospheres with metastable silica-nanonetwork and confined phenyl for simple fabrication of high-surface-area microporous carbon materials. *Carbon* **2020**, *170*, 658−665.

(38) Wang, D.; Kan, Y.; Yu, X.; Liu, J.; Song, L.; Hu, Y. In situ loading ultra-small Cu2O nanoparticles on 2D hierarchical TiO2-graphene oxide dual-nanosheets: Towards reducing fire hazards of unsaturated polyester resin. *J. Hazard. Mater.* **2016**, *320*, 504−512.

(39) Omrani, A.; Afsar, S.; Safarpour, M. A. Thermoset nanocomposites using hybrid nano TiO2−SiO2. *Mater. Chem. Phys.* **2010**, *122*, 343−349.

(40) Wei, Y.-X.; Deng, C.; Chen, H.; Wan, L.; Wei, W.-C.; Wang, Y.-Z. Novel Core−Shell Hybrid Nanosphere towards the Mechanical Enhancement and Fire Retardance of Polycarbonate. *ACS Appl. Mater. Interfaces* **2018**, *10*, 28036−28050.

(41) Wei, Y.-X.; Deng, C.; Wei, W.-C.; Chen, H.; Wang, Y.-Z. Hybrid Nanorods Composed of Titanium, Silicon, and Organophosphorus as Additives for Flame-Retardant Polycarbonate. *ACS Appl. Nano Mater.* **2019**, *2*, 4859−4868.

(42) Wang, X.; Zhou, S.; Guo, W.-W.; Wang, P.-L.; Xing, W.; Song, L.; Hu, Y. Renewable Cardanol-Based Phosphate as a Flame Retardant Toughening Agent for Epoxy Resins. *ACS Sustainable Chem. Eng.* **2017**, *5*, 3409−3416.

(43) Sahoo, S. K.; Khandelwal, V.; Manik, G. Renewable Approach To Synthesize Highly Toughened Bioepoxy from Castor Oil Derivative−Epoxy Methyl Ricinoleate and Cured with Biorenewable Phenalkamine. *Ind. Eng. Chem. Res.* **2018**, *57*, 11323−11334.

(44) Chu, F.; Ma, C.; Zhang, T.; Xu, Z.; Mu, X.; Cai, W.; Zhou, X.; Ma, S.; Zhou, Y.; Hu, W.; Song, L. Renewable vanillin-based flame retardant toughening agent with ultra-low phosphorus loading for the fabrication of high-performance epoxy thermoset. *Compos. Part B: Eng.* **2020**, *190*, No. 107925.

(45) Kumar, S.; Samal, S. K.; Mohanty, S.; Nayak, S. K. Epoxidized Soybean Oil-Based Epoxy Blend Cured with Anhydride-Based Cross-Linker: Thermal and Mechanical Characterization. *Ind. Eng. Chem. Res.* **2017**, *56*, 687−698.

(46) l'Abee, R.; Goossens, H.; Duin, M. V.; Spoelstra, A. Sub-micrometer thermoplastic vulcanizates obtained by reaction-induced phase separation of miscible mixtures of poly(ethylene) and alkyl methacrylates. *Eur. Polym. J.* **2009**, *45*, 503−514.

(47) Vidal, F.; Watson, E. M.; Chen, E. Y. X. All-Methacrylic Stereoregular Triblock Co-polymer Thermoplastic Elastomers Toughened by Supramolecular Stereocomplexation. *Macromolecules* **2019**, *52*, 7313−7323.

(48) Ding, W.; Robertson, M. L. Sustainable thermoplastic elastomers with a transient network. *Eur. Polym. J.* **2019**, *113*, 411−423.

(49) Ballard, N.; Aguirre, M.; Simula, A.; Agirre, A.; Leiza, J. R.; Asua, J. M.; van Es, S. New Class of Alkoxyamines for Efficient Controlled Homopolymerization of Methacrylates. *ACS Macro Lett.* **2016**, *5*, 1019−1022.

(50) Girard, M.; Vidal, D.; Bertrand, F.; Tavares, J. R.; Heuzey, M.-C. Evidence-based guidelines for the ultrasonic dispersion of cellulose nanocrystals. *Ultrason. Sonochem.* **2021**, *71*, No. 105378.

(51) Tajbakhsh, S.; Hajiali, F.; Marić, M. Nitroxide-Mediated Miniemulsion Polymerization of Bio-Based Methacrylates. *Ind. Eng. Chem. Res.* **2020**, *59*, 8921−8936.

(52) Wu, Q.; Hu, Y.; Tang, J.; Zhang, J.; Wang, C.; Shang, Q.; Feng, G.; Liu, C.; Zhou, Y.; Lei, W. High-Performance Soybean-Oil-Based Epoxy Acrylate Resins: "Green" Synthesis and Application in UV-Curable Coatings. *ACS Sustainable Chem. Eng.* **2018**, *6*, 8340−8349.

(53) Ma, Y.; He, L.; Jia, M.; Zhao, L.; Zuo, Y.; Hu, P. Cage and linear structured polysiloxane/epoxy hybrids for coatings: Surface property and film permeability. *J. Colloid Interface Sci.* **2017**, *500*, 349−357.

(54) Lin, X.-B.; Du, S.-L.; Long, J.-W.; Chen, L.; Wang, Y.-Z. A Novel Organophosphorus Hybrid with Excellent Thermal Stability: Core−Shell Structure, Hybridization Mechanism, and Application in Flame Retarding Semi-Aromatic Polyamide. *ACS Appl. Mater. Interfaces* **2016**, *8*, 881−890.

(55) Hajiali, F.; Shojaei, A. Silane functionalization of nanodiamond for polymer nanocomposites-effect of degree of silanization. *Colloids Surf. A Physicochem. Eng. Asp.* **2016**, *506*, 254−263.

(56) Murashkevich, A. N.; Lavitskaya, A. S.; Barannikova, T. I.; Zharskii, I. M. Infrared absorption spectra and structure of TiO 2-SiO 2 composites. *J. Appl. Spectrosc.* **2008**, *75*, 730.

(57) Wen, J.; Li, X.; Li, H.; Ma, S.; He, K.; Xu, Y.; Fang, Y.; Liu, W.; Gao, Q. Enhanced visible-light H2 evolution of g-C3N4 photo-catalysts via the synergetic effect of amorphous NiS and cheap metal-free carbon black nanoparticles as co-catalysts. *Appl. Surf. Sci.* **2015**, *358*, 204−212.

(58) Katoch, A.; Burkhart, M.; Hwang, T.; Kim, S. S. Synthesis of polyaniline/TiO2 hybrid nanoplates via a sol−gel chemical method. *Chem. Eng. J.* **2012**, *192*, 262−268.

(59) Chen, C.; Zhang, N.; He, Y.; Liang, B.; Ma, R.; Liu, X. Controllable Fabrication of Amorphous Co—Ni Pyrophosphates for Tuning Electrochemical Performance in Supercapacitors. *ACS Appl. Mater. Interfaces* **2016**, *8*, 23114−23121.

(60) Ensafi, A. A.; Khoddami, E.; Nabiyan, A.; Rezaei, B. Study the role of poly(diethyl aminoethyl methacrylate) as a modified and grafted shell for TiO2 and ZnO nanoparticles, application in flutamide delivery. *React. Funct. Polym.* **2017**, *116*, 1−8.

(61) Bartolomei, S. S.; Santana, J. G.; Valenzuela Díaz, F. R.; Kavaklı, P. A.; Guven, O.; Moura, E. A. B. Investigation of the effect of titanium dioxide and clay grafted with glycidyl methacrylate by gamma radiation on the properties of EVA flexible films. *Radiat. Phys. Chem.* **2020**, *169*, 107973.

(62) Biswas, M. C.; Jeelani, S.; Rangari, V. Influence of biobased silica/carbon hybrid nanoparticles on thermal and mechanical properties of biodegradable polymer films. *Compos. Commun.* **2017**, *4*, 43−53.

(63) Chen, J.-H.; Yang, M.-C. Preparation and characterization of nanocomposite of maleated poly (butylene adipate-co-terephthalate) with organoclay. *Mater. Sci. Eng. C* **2015**, *46*, 301−308.

(64) Hajiali, F.; Shojaei, A. Network structure and mechanical properties of polydimethylsiloxane filled with nanodiamond − Effect of degree of silanization of nanodiamond. *Compos. Sci. Technol.* **2017**, *142*, 227−234.

(65) Hajiali, F.; Métafiot, A.; Benitez-Ek, L.; Alloune, L.; Marić, M. Nitroxide mediated polymerization of sustainably sourced isobornyl methacrylate and tridecyl methacrylate with acrylonitrile co-monomer. *J. Polym. Sci., Part A: Polym. Chem.* **2018**, *56*, 2422−2436.

(66) Jin, J. M.; Lee, J. M.; Ha, M. H.; Lee, K.; Choe, S. Highly crosslinked poly(glycidyl methacrylate-co-divinyl benzene) particles by precipitation polymerization. *Polymer* **2007**, *48*, 3107−3115.

(67) Grubbs, R. B.; Dean, J. M.; Bates, F. S. Methacrylic Block Copolymers through Metal-Mediated Living Free Radical Polymer-ization for Modification of Thermosetting Epoxy. *Macromolecules* **2001**, *34*, 8593−8595.

(68) Rebizant, V.; Venet, A.-S.; Tournilhac, F.; Girard-Reydet, E.; Navarro, C.; Pascault, J.-P.; Leibler, L. Chemistry and Mechanical Properties of Epoxy-Based Thermosets Reinforced by Reactive and Nonreactive SBMX Block Copolymers. *Macromolecules* **2004**, *37*, 8017−8027.

(69) Hansen, C. M., *Hansen solubility parameters: a user's handbook.* CRC press: 2007.

(70) Lu, L.; Zhou, Z.; Zhang, Y.; Wang, S.; Zhang, Y. Reinforcement of styrene−butadiene−styrene tri-block copolymer by multi-walled carbon nanotubes via melt mixing. *Carbon* **2007**, *45*, 2621−2627.

(71) Loos, J.; Sourty, E.; Lu, K.; de With, G.; Bavel, S. V. Imaging Polymer Systems with High-Angle Annular Dark Field Scanning Transmission Electron Microscopy (HAADF−STEM). *Macromole-cules* **2009**, *42*, 2581−2586.

(72) Treat, N. D.; Varotto, A.; Takacs, C. J.; Batara, N.; Al-Hashimi, M.; Heeney, M. J.; Heeger, A. J.; Wudl, F.; Hawker, C. J.; Chabinyc, M. L. Polymer-Fullerene Miscibility: A Metric for Screening New Materials for High-Performance Organic Solar Cells. *J. Am. Chem. Soc.* **2012**, *134*, 15869−15879.

(73) Jinnai, H.; Higuchi, T.; Zhuge, X.; Kumamoto, A.; Batenburg, K. J.; Ikuhara, Y. Three-Dimensional Visualization and Character-ization of Polymeric Self-Assemblies by Transmission Electron Microtomography. *Acc. Chem. Res.* **2017**, *50*, 1293−1302.

(74) Kalow, J. A.; Swager, T. M. Synthesis of Miktoarm Branched Conjugated Copolymers by ROMPing In and Out. *ACS Macro Lett.* **2015**, *4*, 1229−1233.

(75) He, R.; Zhan, X.; Zhang, Q.; Chen, F. Toughening of an epoxy thermoset with poly [styrene-alt-(maleic acid)]-block-polystyrene-block-poly (n-butyl acrylate) reactive core−shell particles. *RSC Adv.* **2016**, *6*, 35621−35627.

(76) Guo, Y.; Harirchian-Saei, S.; Izumi, C. M. S.; Moffitt, M. G. Block Copolymer Mimetic Self-Assembly of Inorganic Nanoparticles. *ACS Nano* **2011**, *5*, 3309−3318.

(77) Thurber, C.; Gu, L.; Myers, J. C.; Lodge, T. P.; Macosko, C. W. Toughening polylactide with a catalyzed epoxy-acid interfacial reaction. *Polym. Eng. Sci.* **2018**, *58*, 28−36.

(78) Ruiz-Pérez, L.; Royston, G. J.; Fairclough, J. P. A.; Ryan, A. J. Toughening by nanostructure. *Polymer* **2008**, *49*, 4475−4488.

(79) Rebizant, V.; Abetz, V.; Tournilhac, F.; Court, F.; Leibler, L. Reactive Tetrablock Copolymers Containing Glycidyl Methacrylate. Synthesis and Morphology Control in Epoxy−Amine Networks. *Macromolecules* **2003**, *36*, 9889−9896.

(80) Grubbs, R. B.; Dean, J. M.; Broz, M. E.; Bates, F. S. Reactive Block Copolymers for Modification of Thermosetting Epoxy. *Macromolecules* **2000**, *33*, 9522−9534.

(81) Lequieu, J.; Magenau, A. J. D. Reaction-induced phase transitions with block copolymers in solution and bulk. *Polym. Chem.* **2021**, *12*, 12−28.

(82) Serrano, E.; Tercjak, A.; Kortaberria, G.; Pomposo, J. A.; Mecerreyes, D.; Zafeiropoulos, N. E.; Stamm, M.; Mondragon, I. Nanostructured thermosetting systems by modification with epoxidized styrene− butadiene star block copolymers. Effect of epoxidation degree. *Macromolecules* **2006**, *39*, 2254−2261.

(83) Garate, H.; Morales, N.; Goyanes, S.; D'Accorso, N. Miscibility, Phase Separation, and Mechanism of Phase Separation of Epoxy/ Block-Copolymer Blends. *Handbook of Epoxy Blends* 2015, 1 −41.

(84) Argon, A. S.; Cohen, R. E.; Mower, T. M. Mechanisms of toughening brittle polymers. *Mater. Sci. Eng., A* **1994**, *176*, 79−90.

(85) Pearson, R. A.; Yee, A. F. Toughening mechanisms in elastomer-modified epoxies. *J. Mater. Sci.* **1986**, *21*, 2475−2488.

(86) Kissinger, H. E. Variation of Pedk Temperature With Hedting Rote in Differentidl Thermal Andlysis. *J. Res. Natl. Bur. Stand.* **1956**, *57*, 217.

(87) Kissinger, H. E. Reaction kinetics in differential thermal analysis. *Anal. Chem.* **1957**, *29*, 1702−1706.

(88) Chen, Y.; Wang, Q. Thermal oxidative degradation kinetics of flame-retarded polypropylene with intumescent flame-retardant master batches in situ prepared in twin-screw extruder. *Polym. Degrad. Stabil.* **2007**, *92*, 280−291.

(89) Yao, F.; Wu, Q.; Lei, Y.; Guo, W.; Xu, Y. Thermal decomposition kinetics of natural fibers: Activation energy with dynamic thermogravimetric analysis. *Polym. Degrad. Stabil.* **2008**, *93*, 90−98.

(90) Mittal, A.; Garg, S.; Bajpai, S. Thermal decomposition kinetics and properties of grafted barley husk reinforced PVA/starch composite films for packaging applications. *Carbohydr. Polym.* **2020**, *240*, No. 116225.

(91) Saladino, M. L.; Motaung, T. E.; Luyt, A. S.; Spinella, A.; Nasillo, G.; Caponetti, E. The effect of silica nanoparticles on the morphology, mechanical properties and thermal degradation kinetics of PMMA. *Polym. Degrad. Stabil.* **2012**, *97*, 452−459.

(92) Nonahal, M.; Rastin, H.; Saeb, M. R.; Sari, M. G.; Moghadam, M. H.; Zarrintaj, P.; Ramezanzadeh, B. Epoxy/PAMAM dendrimer-modified graphene oxide nanocomposite coatings: Nonisothermal cure kinetics study. *Prog. Org. Coat.* **2018**, *114*, 233−243.

(93) Zabihi, O.; Khodabandeh, A.; Mostafavi, S. M. Preparation, optimization and thermal characterization of a novel conductive thermoset nanocomposite containing polythiophene nanoparticles using dynamic thermal analysis. *Polym. Degrad. Stabil.* **2012**, *97*, 3−13.

(94) Mohammady, S. Z.; Mansour, A. A.; von Soden, W. Effect of Crosslinking on Block and Random Copolymers of Styrene and Butadiene. *Macromol. Chem. Phys.* **2001**, *202*, 2732−2741.

(95) Wang, H. P.; Chum, S. P.; Hiltner, A.; Baer, E. Comparing elastomeric behavior of block and random ethylene−octene copolymers. *J. Appl. Polym. Sci.* **2009**, *113*, 3236−3244.

(96) Speckhard, T. A.; Cooper, S. L. Ultimate tensile properties of segmented polyurethane elastomers: factors leading to reduced properties for polyurethanes based on nonpolar soft segments. *Rubber Chem. Technol.* **1986**, *59*, 405−431.

(97) Lee, J. M.; Kim, J.-S.; Cheong, I. W.; Kim, J. H. Synthesis, characterization, and mechanical property of poly(urethane-glycidyl methacrylate-methyl methacrylate) hybrid polymers. *J. Appl. Polym. Sci.* **2011**, *121*, 3111−3121.

(98) Wan, Y.-J.; Tang, L.-C.; Gong, L.-X.; Yan, D.; Li, Y.-B.; Wu, L.-B.; Jiang, J.-X.; Lai, G.-Q. Grafting of epoxy chains onto graphene oxide for epoxy composites with improved mechanical and thermal properties. *Carbon* **2014**, *69*, 467−480.

(99) Bortz, D. R.; Heras, E. G.; Martin-Gullon, I. Impressive Fatigue Life and Fracture Toughness Improvements in Graphene Oxide/ Epoxy Composites. *Macromolecules* **2012**, *45*, 238−245.

(100) Shi, S.; Shen, D.; Xu, T.; Zhang, Y. Thermal, optical, interfacial and mechanical properties of titanium dioxide/shape memory polyurethane nanocomposites. *Compos. Sci. Technol.* **2018**, *164*, 17−23.

(101) Buxton, G. A.; Balazs, A. C. Lattice spring model of filled polymers and nanocomposites. *J. Chem. Phys.* **2002**, *117*, 7649−7658.

(102) Sarkar, B.; Alexandridis, P. Block copolymer−nanoparticle composites: Structure, functional properties, and processing. *Prog. Polym. Sci.* **2015**, *40*, 33−62.

(103) Leyva, M. E.; Soares, B. G.; Khastgir, D. Dynamic-mechanical and dielectric relaxations of SBS block copolymer: polyaniline blends prepared by mechanical mixing. *Polymer* **2002**, *43*, 7505−7513.

(104) Liu, J. (. D.).; Thompson, Z. J.; Sue, H.-J.; Bates, F. S.; Hillmyer, M. A.; Dettloff, M.; Jacob, G.; Verghese, N.; Pham, H. Toughening of Epoxies with Block Copolymer Micelles of Wormlike Morphology. *Macromolecules* **2010**, *43*, 7238−7243.

(105) Berglund, C. A.; McKay, K. W. Viscoelastic properties of a styrene-isoprene-styrene triblock copolymer and its blends with polyisoprene homopolymer and styrene-isoprene diblock copolymer. *Polym. Eng. Sci.* **1993**, *33*, 1195−1203.

(106) Kraus, G.; Rollmann, K. W. The entanglement plateau in the dynamic modulus of rubbery styrene−diene block copolymers. Significance to pressure-sensitive adhesive formulations. *J. Appl. Polym. Sci.* **1977**, *21*, 3311−3318.

(107) Wu, C.-J.; Gaharwar, A. K.; Chan, B. K.; Schmidt, G. Mechanically Tough Pluronic F127/Laponite Nanocomposite Hydrogels from Covalently and Physically Cross-Linked Networks. *Macromolecules* **2011**, *44*, 8215−8224.

(108) Martin, J. E.; Patil, A. J.; Butler, M. F.; Mann, S. Guest-Molecule-Directed Assembly of Mesostructured Nanocomposite Polymer/Organoclay Hydrogels. *Adv. Funct. Mater.* **2011**, *21*, 674−681.

(109) Mishra, J. K.; Hwang, K.-J.; Ha, C.-S. Preparation, mechanical and rheological properties of a thermoplastic polyolefin (TPO)/ organoclay nanocomposite with reference to the effect of maleic anhydride modified polypropylene as a compatibilizer. *Polymer* **2005**, *46*, 1995−2002.

(110) Esposito, L. H.; Ramos, J. A.; Kortaberria, G. Dispersion of carbon nanotubes in nanostructured epoxy systems for coating application. *Prog. Org. Coat.* **2014**, *77*, 1452−1458.

(111) Xu, C.; Ohno, K.; Ladmiral, V.; Composto, R. J. Dispersion of polymer-grafted magnetic nanoparticles in homopolymers and block copolymers. *Polymer* **2008**, *49*, 3568−3577.

(112) Lan, Q.; Francis, L. F.; Bates, F. S. Silica nanoparticle dispersions in homopolymer versus block copolymer. *J. Polym. Sci. B Polym. Phys.* **2007**, *45*, 2284−2299.

(113) Konwar, U.; Das, G.; Karak, N. Mesua ferrea L. seed oil based highly branched polyester/epoxy blends and their nanocomposites. *J. Appl. Polym. Sci.* **2011**, *121*, 1076−1085.

(114) Toledo, L.; Palacio, D. A.; Urbano, B. F. Tuning the softness of poly(2-hydroxyethyl methacrylate) nanocomposite hydrogels through the addition of PEG coated nanoparticles. *J. Colloid Interface Sci.* **2020**, *578*, 749−757.